



Article

Cite this article: Toyota T, Ono T, Tanikawa T, Wongpan P, Nomura D (2020). Solidification effects of snowfall on sea-ice freeze-up: results from an onsite experimental study. *Annals of Glaciology* **61**(83), 299–308. <https://doi.org/10.1017/aog.2020.49>

Received: 27 September 2019

Revised: 14 June 2020

Accepted: 15 June 2020

First published online: 14 July 2020

Key words:



Crystal alignments; freeze-up process; snowfall effect; surface heat budget; thermodynamic ice growth model; thin sea ice

Author for correspondence:

Takenobu Toyota,

E-mail: toyota@lowtem.hokudai.ac.jp

Solidification effects of snowfall on sea-ice freeze-up: results from an onsite experimental study

Takenobu Toyota¹ , Takashi Ono², Tomonori Tanikawa³, Pat Wongpan^{1,4} 
and Daiki Nomura^{5,6,7,8}

¹Institute of Low Temperature Science, Hokkaido University, Sapporo, Hokkaido, Japan; ²Graduate School of Environmental Sciences, Hokkaido University, Sapporo, Hokkaido, Japan; ³Meteorological Research Institute, Japan Meteorological Agency, Tsukuba, Ibaraki, Japan; ⁴JSPS International Research Fellow, Japan Society for the Promotion of Science, Tokyo, Japan; ⁵Faculty of Fisheries Sciences, Hokkaido University, Hakodate, Hokkaido, Japan; ⁶Arctic Research Center, Hokkaido University, Sapporo, Hokkaido, Japan; ⁷Global Station for Arctic Research, Global Institution for Collaborative Research and Education, Hokkaido University, Sapporo, Hokkaido, Japan and ⁸Hokkaido University Field Science Center for Northern Biosphere

Abstract

Although the effects of snow during sea-ice growth have been investigated for sea ice which is thick enough to accommodate dry snow, those for thin sea ice have not been paid much attention due to the difficulty in observing them. Observations are complicated by the presence of slush and its subsequent freeze-up, and the surface heat budget might be sensitive to the additional ice thickness. An onsite short-term land fast sea-ice freeze-up experiment in the Saroma-ko Lagoon, Hokkaido, Japan was carried out to examine the effects of snowfall on the structure and surface heat budget of thin sea ice, based on observational results and a 1-D thermodynamic model. We found that snowfall contributes to the solidification of the surface slush layer, contributing ice thickness that is comparable to the snowfall amount and affecting the crystal texture significantly. On the other hand, the basal ice growth rate and turbulent heat flux were not significantly affected, being $<3.1 \times 10^{-8} \text{ m s}^{-1}$ and 3 W m^{-2} , respectively. This finding may validate the omission in past studies of snow effect in estimating ice production rates in polynyas and has implications about the reconstruction of growth history from sample analysis.

1. Introduction

The accumulation of snow on sea ice plays an important role in modifying the properties of sea ice in several ways. With respect to sea-ice growth and the surface heat budget, the thermal insulation effect and process of snow-ice formation have mainly been investigated for sea ice that is thick enough to accumulate snow as a dry layer on top (e.g. Holtzmark, 1955; Fichet and Maqueda, 1999; Wu and others, 1999; Fichet and others, 2000; Maksym and Jeffries, 2000; Jutras and others, 2016; Sturm and Massom, 2017). On the other hand, the effect on the freeze-up process of thin sea ice, complicated by the formation of slush containing sea water exposed to the air, is not fully understood due to the lack of observations. Snowfall on a wet, thin sea-ice surface can potentially affect the production rate and subsequent crystal alignment through the seeding effect which induces crystallization (Martin, 1981; Gow, 1986; Weeks and Ackley, 1986; Svensson and Omstedt, 1994). Besides, the addition of ice thickness due to the incorporation of a surface slush layer may reduce the heat exchange with the atmosphere considerably (Maykut, 1978). Although traditionally the effect of snow has been omitted when estimating the sea-ice production rate in polynyas (e.g. Pease, 1987; Martin and others, 1998; Tamura and others, 2008), this decision seems to have been for simplicity rather than based on observational facts and can give rise to large uncertainty in the computation (Spreen and Kern, 2017).

Observational studies on thin ice growth processes have been relatively limited due to logistical difficulties (e.g. Gow and others, 1990; Perovich and Richter-Menge, 2000; Wettlaufer and others, 2000; Granskog and others, 2004), and focused on the relationship between the heat budget and entrapped brine or chemical properties. Although Gow and others (1990) did explore the contribution of wind-blown snow from perennial ice to snow-ice formation using a transect measurement across Arctic leads, we still need more detailed data to better understand and quantify the effect of snow. Fortunately, we had the opportunity to observe the effect of snow on the crystal textures and growth of thin sea ice from field experiments at the Saroma-ko Lagoon, Hokkaido, Japan (Fig. 1). To our knowledge, this experiment and resulting data are novel.

The stability of the field site on the Saroma-ko Lagoon makes it very suitable investigating this issue. Accordingly, there have already been several experiments targeting thin ice and snow, examining its growth rate (Hasemi, 1974), the salinity evolution associated with snow-ice formation (Takizawa and Wakatsuchi, 1982; Takizawa, 1983, 1984), the surface heat budget on sea ice (Ishikawa and Kobayashi, 1984) and the upward brine migration in sea ice (Kasai and Ono, 1984). However, few studies addressed the effect of snowfall on the

© The Author(s), 2020. Published by Cambridge University Press. This is an Open Access article, distributed under the terms of the Creative Commons Attribution licence (<http://creativecommons.org/licenses/by/4.0/>), which permits unrestricted re-use, distribution, and reproduction in any medium, provided the original work is properly cited.

cambridge.org/aog



Fig. 1. Map of the Saroma-ko Lagoon and the experiment site. The locations of the ALMO and the Tokoro automated meteorological station are also shown.

crystal alignment and surface heat budget for thin sea ice. Although Kawamura (1982) investigated the evolution of crystallographic orientations in thin sea ice, the effect of snow was not considered. And although similar experiments were conducted at a comparatively stable site in the Baltic Sea (Granskog and others, 2004), their focus was on the behavior of chemical components.

The purpose of this paper is to present a case study that quantitatively estimates the effects of snowfall on ice structure and heat exchange with the atmosphere during the freeze-up process of thin sea ice. These estimates are based on results obtained from artificial pool experiments and a traditional 1-D thermodynamic sea-ice growth model. The model is based on a simple surface heat balance investigation (Maykut and Untersteiner, 1971; Semtner, 1976; Maykut, 1978) and was used to estimate the effect of snow on ice growth and the individual heat fluxes at the ice surface. Since snow relates partly to the formation of granular ice through snow-ice formation or superimposed ice (e.g. Kawamura and others, 1997), our study seeks to advance understanding about the substructure of granular ice and its impact on ice growth.

2. Observations

The experiment was conducted over two nights from 25 to 27 February in 2019 as part of the Saroma-ko Lagoon Observations for sea-ice Physico-chemistry and Ecosystems 2019 program (SLOPE2019; Nomura and others, 2020). The experiment site was located at 44°07' N, 143°58' E, ~200 m away from the eastern shore of the Saroma-ko Lagoon, Hokkaido, Japan (Fig. 1). The dimensions of the square pool made for this experiment were 1.5 m × 1.5 m (Fig. 2a). The depth and salinity of the sea water in the pool were 1.2 m and 31.2 psu, respectively, and it was surrounded by 0.32 m thick land fast ice with 0.09 m of snow. According to the formula of UNESCO (1978), the freezing temperature (T_f) is estimated to be -1.71°C from the salinity. With the significant wintertime solar radiation at this latitude (Toyota and Wakatsuchi, 2001), our experiment was limited to nighttime when the sea-ice growth occurred.

2.1 Meteorological and ice conditions

Air temperature, relative humidity and sea level pressure were recorded to monitor the meteorological conditions and calculate surface heat fluxes during ice growth. Measurements were performed at a height of 1.5 m at 1-min intervals by an Automatic Weather System (AWS, Kestrel manufacturer) on the Saroma-ko Lagoon (Fig. 2b), mounted 2 km away from the eastern coast of the lake (Nomura and others, 2020). The nominal accuracies of air temperature, relative humidity and wind speed are 0.5°C , 2% and 3% of reading, respectively. The time series of air temperature and wind speed for the experimental period are shown in Figures 3a and b. Air temperature varied from -15 to -3°C with southerly to westerly winds ranging from 0 to 5 m s^{-1} during our experiment. In Figure 3b it is noted that some wind data were partly missing at nighttime, presumably due to the freezing of the anemometer under the cold air (-15 to -10°C) and undersaturated humidity (85–90%) conditions. These data gaps were filled with wind speed measurements from the Tokoro automated meteorological station operated by Japan Meteorological Agency, located ~5 km away from the Saroma-ko Lagoon (Fig. 1). This was justified by the strong agreement between the two sites for daytime measurements.

To assess the upwelling and downwelling radiative fluxes, shortwave (305–2800 nm) and longwave (3–50 μm) radiation was monitored every minute with a radiometer (EKO Instruments Co., Ltd., MR-40) with the accuracy of ~1–2% of the measured values. The radiometer was mounted on the snow surface near the AWS to avoid impacting the freezing conditions in the pool (Fig. 2b). The time series of each radiative flux, together with net flux, are shown in Figure 3c. The coupled variation of the downwelling longwave radiation and shortwave radiation likely indicates the presence/absence of clouds. Hence, it is inferred that the weather during the experiments was fair but occasionally cloudy for the first night (25–26 February) whereas mostly cloudy for the second night (26–27 February). The net radiative flux was positive (up to 150 W m^{-2}) from 06:00 to 15:00 whereas it became close to zero or negative from ~15:00 through to the early morning of the next day. Due to the quite different surface conditions between the radiometer site (snow surface) and pool site (thin ice), the upwelling longwave radiative flux used for the model was calculated from the Stefan–Boltzmann law (refer to Section 3.2 for details).

To monitor the freezing conditions, vertical temperature profiles of the air and water near the surface (at 0.01, 0.06 and 0.22 m above the water and at the depths of 0.03 and 0.20 m) were recorded at one corner of the pool (Fig. 2a) during the observation, using five thermo-recorders (RT-32S from ESPEC MIC Corporation), with a measurement accuracy of 0.1°C . The time series of water temperatures at depths of 0.03 and 0.20 m are shown in Figure 4. Although temperatures at both depths increased by $\sim 0.5^\circ\text{C}$ in the daytime through the absorption of solar radiation into the water, they began to decrease after 15:00 and remained close to the freezing point (-1.7°C) from 18:00 to 06:00 through the night. This is consistent with the diurnal variation of the net radiative flux in Figure 3c, where the net radiative flux became negative at ~15:00 on both days, and therefore it is likely that the solar heat absorbed into the water during the daytime was completely released back into the air by 18:00 on both days. Based on this result, we presumed that sea-ice formation began at 18:00 and the sensible heat flux from the underlying water was not taken into account in the thermodynamic model.

The ice conditions and snowfall events at the pool site were monitored at 1-min intervals from 07:00 to 17:00 on each day with a camera mounted near the pool (Fig. 2a). To detect snowfall events each night, we referred to records at the Abashiri Local

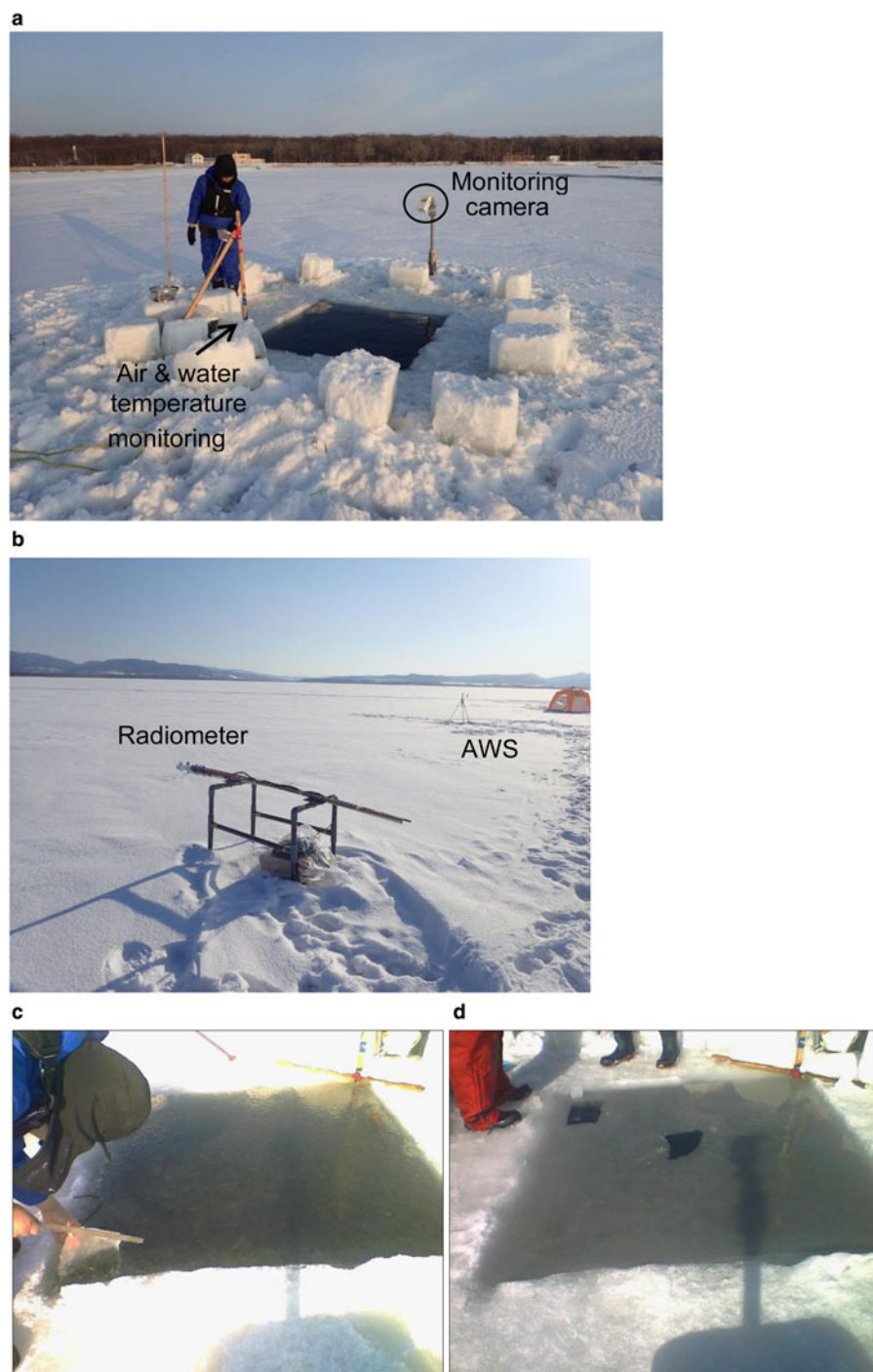


Fig. 2. Photographs of our experiments at an artificial pool site to examine how meteorological conditions affect sea-ice properties at the early growth stage. (a) Pool site with a dimension of 1.5 m \times 1.5 m. Ice conditions were monitored with a monitoring camera. Air and water temperature near the ice surface were monitored with a thermistor at the corner of the pool. (b) Photo showing the setup of our radiometer and AWS. (c) Photo of ice conditions at the sampling time at 09:26 on 26 February and (d) same as (c) except for at 09:38 on 27 February, taken by a monitoring camera in Figure 2a. Note that there is no snow layer on sea ice.

Meteorological Observatory (ALMO), located \sim 25 km east of the site, and the hourly snow data from the Tokoro station (Fig. 1). According to the monitoring camera photos at the pool, light snowfall events occurred at 13:05–13:20, 14:38–15:25 and 16:04–17:00 on 26 February during the observation period. However, based on the following observational facts, we infer that there was no significant snowfall except for during 19:30–20:30 on 26 February for the second night, when snowfall accumulated in a 0.01 m thick layer at the pool:

- (1) The document at ALMO reported that a significant snowfall with visibility $<$ 2 km was limited to 30 min duration between 20:40 and 21:10 and it resulted in a 0.01 m thick layer during 20:00–21:00 on 26 February.
- (2) No snowfall was recorded at either Tokoro or Abashiri except for the above period.

- (3) According to Figures 3c and 6b, net longwave radiation was close to zero from 19:30–20:30 on 26 February, indicating thick clouds cover over this area during this period.
- (4) Snow pit measurements conducted on the Saroma-ko Lagoon on the morning of 27 February revealed a 0.01 m thick new snow layer on top of the pre-existing snow layer (Table 1).

2.2 Sea-ice sampling

The newly formed sea ice of \sim 2–3 cm thickness was collected at 09:26 on 26 February and at 09:38 on 27 February (Local time) by cutting out an area of 0.15 m \times 0.15 m area with a portable saw (Figs 2c and d). As shown in these figures, there was no dry snow layer on the sea ice in the pool at the sampling time. The ice samples were kept in resealable bags that were

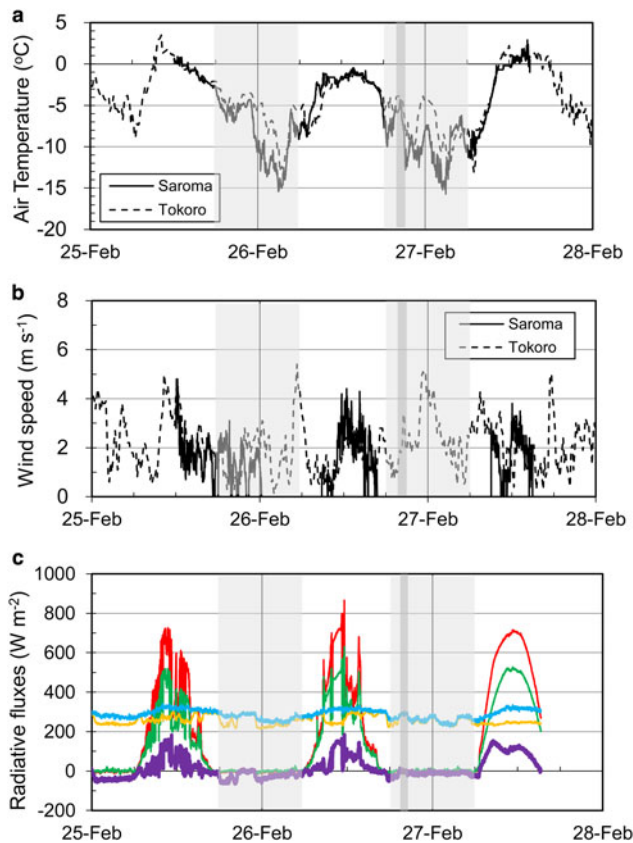


Fig. 3. Meteorological data observed on the Saroma-ko Lagoon with light gray shades showing the ice growth periods (18:00 to 06:00) and dark gray shades showing a snowfall event (19:30 to 20:30 on 26 February). (a) Air temperature with the data at Tokoro (Fig. 1a) in broken line. (b) Wind speed with the data at Tokoro (Fig. 1a) in broken line. (c) Radiative fluxes of downward shortwave (red), upward shortwave (green), downward longwave (orange), upward longwave (blue) and net (purple). Note that radiation data were taken on the snow surface.

immediately stored with coolant (-25°C) in an insulation box, and then sent to the Institute of Low Temperature Science (ILTS), Hokkaido University in Sapporo within the sampling day. They were kept in a cold room at a temperature of -15°C for analysis. Although the ice samples experienced large temperature changes before analysis, this is assumed to have had a negligible impact on the crystal texture and salinity of the ice samples that we were focused on.

3. Analytical method

3.1 Sample analysis

Sea-ice samples were processed in the ILTS cold room at -15°C to carry out thick (5 mm) and thin (1 mm) section analyses for examining the inclusions and crystal alignments, respectively. First, ice samples were vertically sliced to make a 7 mm thick ice section with a bandsaw, and then they were attached onto slightly warmed glass. The samples were placed on dark clothes and photographed with scattered light to observe inclusions. Next, the samples on the glass were sliced carefully with a microtome until the thickness reached 1 mm, and then photos were taken through crossed polarizers to observe crystal alignments.

The salinities of the samples were also measured. Since the two-layered structure was prominent for each sample (Fig. 5), the salinities of the individual layers were measured. To do so, rectangular columns with dimensions of 6 cm \times 6 cm (see Table 2 for individual ice thicknesses) were cut out from the ice samples, and then each column was cut horizontally at

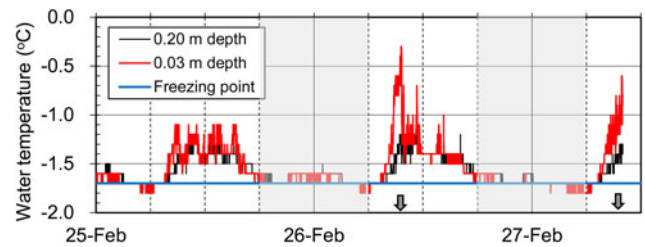


Fig. 4. Time series of water temperature at 0.03 and 0.20 m depths at the pool site with gray shading showing the ice growth periods (18:00 to 06:00). Arrows denote the timings of sample collection.

Table 1. Snow pit measurements

Date and time	Snow depth (m)	Depths (m)	Grain shape	Grain sizes (mm)
25 February; 16:30	0.09	0.07–0.09	RG	0.2–0.4
		0.02–0.07	DH	0.4–1.0
		0.00–0.02	DH and MF	0.6–1.0
27 February; 11:05	0.09	0.08–0.09	PP	0.1–0.2
		0.06–0.08	RG	0.2–0.4
		0.03–0.06	DH	0.4–1.5
		0.00–0.03	DH & MF	0.4–2.0

³In Grain shape, RG, DH, MF and PP denote rounded grains, depth hoar, melt forms and precipitation particles, respectively. Measurements were conducted at the same site on Lake Saroma, close to a radiometer. Mean snow density was $309 \pm 32(\text{sd}) \text{ kg m}^{-3}$. Snow type classification is based upon The International Classification for Seasonal Snow on the Ground (Fierz and others, 2009). Snow temperatures at the heights of 0.00, 0.03, 0.06 and 0.09 m from the snow/ice boundary were -3.1 , -2.6 , -2.5 and -2.6°C , respectively, on 25 February, and -3.4 , -2.9 , -2.7 and -2.5°C , respectively, on 27 February.

the depth of the boundary between the two layers. Salinities were measured with a salinometer (WTW Cond 3110, nominal accuracy: 0.1 psu) after melting the ice samples at room temperature. The results are listed in Table 2. The averaged salinities of the granular and columnar ice layers are 10.4 and 10.2 psu, respectively. There was no significant difference between these two ice types or sampling dates. These values are comparable with the 12 psu reported by Takizawa (1984) for snow ice formed in the pool at the Saroma-ko Lagoon. The reason for the lack of salinity contrast between these two layers seems to be because of the increased permeability of sea ice when it is near the freezing point. The brine volume fraction was estimated to be 24–30% using the formula of Frankenstein and Garner (1967) by substituting the model-derived T_s (-2.4 to -1.7°C) and measured bulk salinity (10.2 psu), well above the traditional 5% threshold of permeability (Golden and others, 1998). This enhanced brine drainage induced by increasingly permeable structure, irrespective of ice type, was previously highlighted by Takizawa (1984).

3.2 1-D thermodynamic model

To examine the snow effect quantitatively, we calculated the ice thickness evolution with a thermodynamic ice-growth model used in Toyota and Wakatsuchi (2001). This model is originally based on Maykut (1978) and calculates ice growth from a simple surface heat balance equation expressed by Eqns (1) and (2). Sensible heat flux (FSH) is obtained from $\rho_a c_p C_s u (T_a - T_s)$ with the bulk method, where T_a is the observed air temperature, T_s is the surface temperature of the ice given by solving Eqn (1), ρ_a is the air density (1.3 kg m^{-3}), c_p is the specific heat of the air ($1004 \text{ J kg}^{-1} \text{ K}^{-1}$), C_s is the transfer coefficient for sensible heat and u is the observed wind speed. Latent heat flux (FLH) is obtained from $0.622 \rho L_v C_e u (r e_{sa} - e_{ss})/p$ with the bulk method, where L_v is the latent heat of sublimation ($2.84 \times 10^6 \text{ J kg}^{-1}$; Yen, 1981), C_e is the transfer coefficient for latent heat, r is the observed

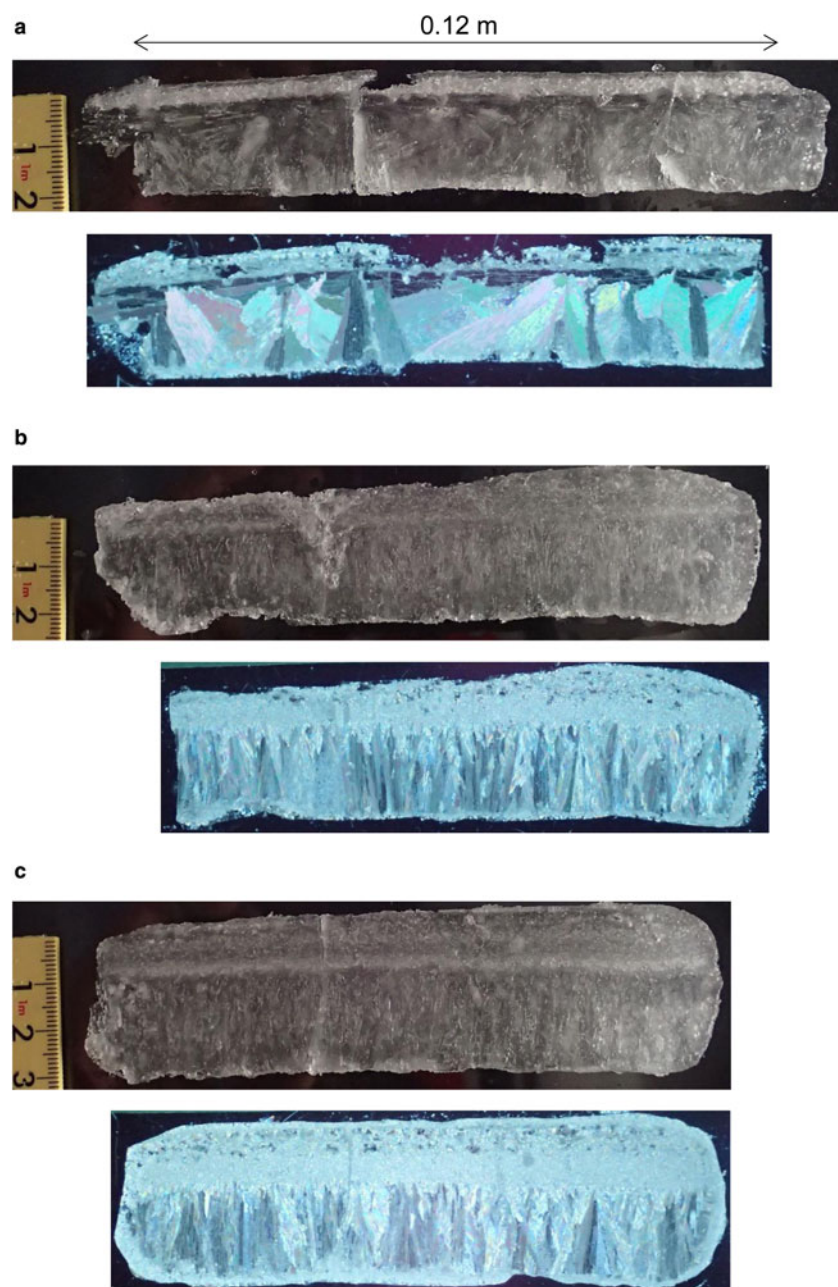


Fig. 5. Vertical structures by thick (5 mm) (upper) and thin (1 mm) (lower) section analysis for sea-ice samples collected at (a) 09:26 on 26 February near the margin of the pool, (b) 09:38 on 27 February near the center of the pool, and (c) 09:38 on 27 February near the margin of the pool. Total ice thicknesses for (a)–(c) are 23, 30 and 35 mm, respectively. In each figure, top of the sample corresponds to the ice surface.

relative humidity, p is the observed surface pressure and e_{sa} and e_{ss} are the saturation vapor pressure in the atmosphere and at the ice surface, respectively. The dependence of e_s on air temperature is expressed as a fourth-order polynomial developed by Maykut (1978). C_s and C_e are taken to be 1.0×10^{-3} after Aota and others (1989).

The downward longwave radiation (FLW_{\downarrow}) was given by the radiometer mounted near the AWS, whereas the outgoing longwave radiation (FLW_{\uparrow}) was calculated by $\varepsilon \sigma T_s^4$, where ε is the emissivity and taken to be 0.97 (Maykut, 1986), and σ is the Stefan–Boltzmann constant because the surface conditions at the pool site were significantly different from those at the radiometer site. Since the penetration depth of longwave radiation is less than a few millimeters (e.g. Bae and others, 2010), there seems no need to consider the penetration fraction of FLW_{\downarrow} . The conductive heat flux in sea ice (FCI) can be written as $k_i(T_B - T_s)/H_i$ on the assumption of the ice being snow-free, where k_i and H_i are the thermal conductivity and thickness of sea ice, respectively. This assumption is justified from the photos at the sampling time (Figs 2c and d). k_i is set to $2.0 \text{ W K}^{-1} \text{ m}^{-1}$ as the representative

value for sea ice at $\sim -2^\circ\text{C}$. T_B is the temperature at the ice bottom and is taken to be $T_f (= -1.71^\circ\text{C})$. T_s is solved using Eqn (1) with the Newton–Raphson method, assuming that all heat fluxes are balanced at the surface thin ice layer:

$$\text{FSH}(T_s) + \text{FLH}(T_s) + \text{FLW}_{\uparrow}(T_s) + \text{FLW}_{\downarrow} + \text{FCI}(T_s) = 0 \quad (1)$$

Thereafter the individual fluxes are calculated by substituting the obtained T_s . The ice growth rate was calculated from the following heat-balance equation at the ice bottom on the assumption of no ocean heat flux

$$\rho_i L_f dH_i/dt = \text{FCI}, \quad (2)$$

where ρ_i is the ice density (900 kg m^{-3}). L_f is the latent heat of fusion and taken to be $2.27 \times 10^5 \text{ J kg}^{-1}$ by substituting the sea-ice salinity (10.2 psu) for congelation ice (Table 2) and the freezing temperature (-1.71°C) into the Yen (1981) formula. The initial ice thicknesses ($0.10 \times 10^{-3} \text{ m}$ and $0.11 \times 10^{-3} \text{ m}$ for the first

Table 2. Salinities of sea-ice samples

Sampling date and location	Depths (mm)	Salinity (psu)	Ice type ^a	
26 February Margin	0–5	10.2	Granular (SSL)	
	5–23	11.6	Dark + columnar (CI)	
27 February Center	0–10	10.5	Granular (SSL)	
	10–30	8.6	Columnar (CI)	
	Margin	0–15	10.6	Granular (SSL)
		15–35	10.4	Columnar (CI)
	Average ± SD	10.4 ± 0.2	Granular (SSL)	
	10.2 ± 1.5	Columnar (CI)		

^aSSL and CI denote surface solidification layer and congelation ice, respectively.

and second nights, respectively) were calculated from the heat loss per second at the water surface at the freezing point at 18:00 on each day, assuming that sea ice began to grow at 18:00. The subsequent ice thickness evolution was obtained by integrating Eqn (2) with a time step of 1 min. The assumption of no ocean heat flux is justified by the fact that the water temperature remained at the freezing point at depths of both 0.03 and 0.20 m in Figure 4.

4. Results

4.1 Sea-ice structure

The vertical thick and thin sections of ice samples are shown in Figure 5. Since the sea-ice samples were collected at the margin and center of the pool site on 27 February, two sections are shown for this day. The thick section structure in Figure 5 clearly shows a layered structure for each sample and the contrast between the two experiments is noticeable. For the 26 February sample, the whitish layer in the top 5 mm is followed by a thin dark layer and then a relatively coarse translucent layer (Fig. 5a), whereas the 27 February sample shows two fine-structured translucent layers separated by a distinct boundary (Figs 5b and c). Correspondingly, the contrast in the crystal alignments for the thin sections from the two experiments is also noticeable for the full depth of the samples. The 26 February sample was composed of granular ice (~5 mm thick), a thin dark layer with a vertical *c*-axis, and columnar ice with a horizontal *c*-axis and large grain size (~18 mm thick in Fig. 5a), whereas the 27 February sample had fine grained granular ice (~10 mm thick in Fig. 5b and 15 mm thick in Fig. 5c) and then much thinner-structured columnar ice. The fine-grained granular ice indicates that this layer formed within a short time. The granular ice in Figure 5c is further divided into the upper 5 mm thick layer and the lower 10 mm thick layer, where the upper layer has somewhat larger grain sizes than the lower layer. The difference in ice thickness between the two samples results from the absence of this upper layer in Figure 5b. The formation process of this layer will be discussed in Section 5.2.

The crystal structure in the thin section of Figure 5a is quite similar to that of the ice grown in the tank experiment under calm conditions by Toyota and others (2013), except for the granular ice at the top (compare with their Fig. 2). This suggests that the sea ice formed under the relatively calm conditions on the first night (25–26 February), was free from any disturbance. On the other hand, the meteorological conditions on the second night likely affected the sea-ice structure during the growth period. Given that the air temperature and wind speed conditions were relatively similar for these two nights (Fig. 3), the key difference was the snowfall event that occurred at ~20:30 on 26 February, as described in Section 2.1. Therefore, it is most likely that the 10 mm thick granular ice layer overlying the columnar ice in Figures 5b and c is attributed to snow-related processes.

It is interesting to note that the thickness of this layer is comparable with the estimated snowfall amount.

4.2 Ice growth and surface heat budget

Here the results from the 1-D thermodynamic model are presented. The ‘no snow’ ice growth calculated each night from 18:00 to 06:00 is shown with a red solid line for the first night and a black solid line for the second night in Figure 6a. We stopped the calculation at 06:00 on the next day because our focus is ice growth at night and the effect of solar radiation cannot be neglected (Fig. 3c), i.e. Eqn (1) does not apply, after 06:00. The ice thickness at 06:00 amounted to 16 mm for 26 February and 17 mm for 27 February. These values are close to the observed thicknesses of columnar ice in Figure 5 (18 ± 1 mm for 26 February and 20 ± 1 mm for 27 February). We confirmed that the difference in the predicted ice thickness caused by the measurement errors of the meteorological observations is within only ±0.5 mm. Considering the possibility of slight growth between 06:00 and the sampling time (~09:30), our calculation closely reproduces the observed ice thickness. The time series of the sensible, latent and net longwave radiative heat fluxes used for calculating the ice growth rate during the first and second nights are shown in Figures 6b and c, respectively, and the averages of the individual fluxes for each night are depicted in Figure 7. These figures indicate that FLW is the dominant heat flux in determining the sea-ice growth rate. The large variation of FLW in Figures 6b and c was caused by the variation of downward longwave radiation, which is controlled mainly by the amount of cloud cover. Thus, cloud cover plays an important role in determining the ice growth rate. The values in Figure 7 are comparable with those of past observations conducted over thin ice at the pool on the Saroma-ko Lagoon by Ishikawa and Kobayashi (1984). These results all indicate that our model reproduced the real ice growth and heat fluxes successfully.

Here, we examine the effect of the solidification of the surface slush layer on the subsequent ice growth and turbulent heat flux with our model, by artificially adding 10 mm to the ice thickness at 21:00 on 26 February on the assumption that this layer formed immediately after the main snowfall event. We continued the ice growth calculation after 21:00 with the same atmospheric forcing for the second night. In this calculation, we used the same k_i for the thermal conductivity of the solidification layer based on the near match in salinity values for the granular ice and columnar ice (Table 2). The temporal evolution of ice thickness is depicted with a broken line in Figure 6a, and the averaged heat fluxes are shown with dotted bars in Figure 7. Figure 6a shows a slight decrease in the sea-ice growth rate after the addition of the solidification layer, compared with the result without it. This is explained by the decrease in T_s (predicted from -2.5°C without snow to -2.9°C with solidification layer at 06:00 on 27 February), which results in the reduction in FSH, FLH and FLW, and the reduction in the vertical temperature gradient in ice (from -46.4 K m⁻¹ without snow to -45.2 K m⁻¹ with solidification layer at 06:00 on 27 February), which are both associated with an addition of ice thickness. Accordingly, the turbulent heat flux (FSH + FLH) released from the ice to the atmosphere is somewhat reduced (Fig. 7). However, the decrease in ice thickness at 06:00 and the reduction in turbulent heat flux (FSH + FLH) is estimated to be <1 mm and 2.5 W m⁻², respectively. These results indicate that the addition of a 10 mm thick solidification layer affected neither ice growth nor surface heat flux significantly.

To confirm our result, we further examined the effect of the solidification of the surface slush layer by changing the layer thickness in our 1-D thermodynamic sea-ice model from 10 to 30 mm, assuming that the formation of this layer would be

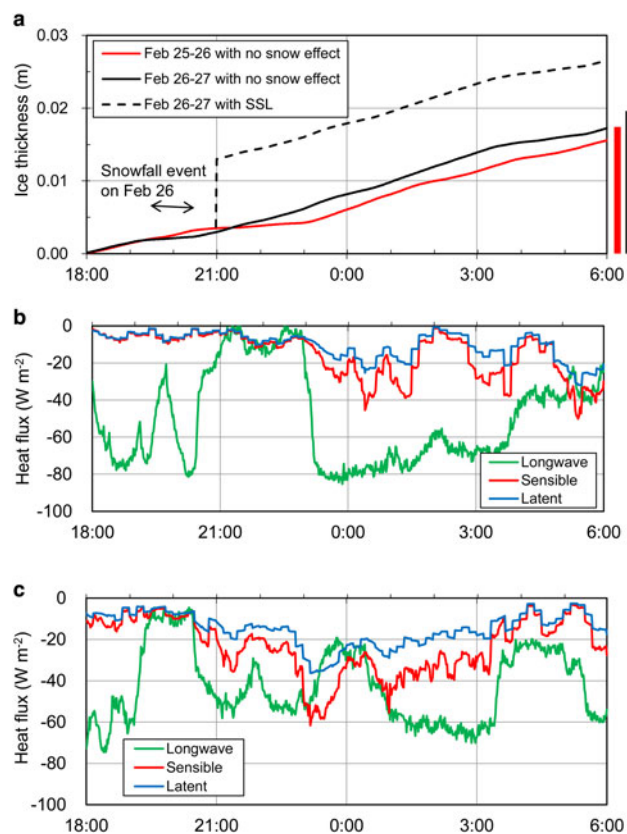


Fig. 6. Sea-ice growth during the nights calculated with a 1-D thermodynamic ice growth model. (a) Temporal evolution of ice thickness. (Red line: without snow for the first night, black solid line: without snow for the second night and black broken line: for the second night, including the surface solidification layer (SSL).) Two bars ~06:00 denote the real columnar ice thickness observed in the ice samples. (Red bar: 26 February and black bar: 27 February.) (b) Temporal variation of individual heat fluxes during the first night (25–26 February). (Green: net longwave radiation, red: sensible heat flux and blue: latent heat flux.) Note that net longwave radiation was obtained by summing up the downward flux observed by the radiometer and the upward flux calculated by the model. (c) Same as (b) except for during the second night (26–27 February).

limited to less than a few centimeters because of large amount of heat flux needed to form it (Section 5.1). Figure 8a shows the temporal evolution of the additional ice thickness from 21:00 on 26 February until 06:00 on 27 February for each solidification layer thickness. The corresponding averaged heat fluxes of FSH, FLH and FLW are depicted in Figure 8b. These figures show that although both ice thickness growth and turbulent heat flux decrease in association with the increase in the thickness of the solidification layer at 10, 20 and 30 mm only resulted in a 0.7, 1.3 and 1.8 mm decrease in ice thickness (<11% of the total thickness), respectively, and only 3, 5 and 7 W m^{-2} decrease for turbulent heat flux (<15% of total flux). This indicates that the solidification of the surface slush layer during the freeze-up process does not have a significant effect on the subsequent ice growth and turbulent heat flux for snowfall amounts less than a few centimeters. This result may justify the omission of snow effects, as far as snowfall amount is less than a few centimeters, in estimating the ice production rates or heat fluxes in the polynyas by the past studies (e.g. Pease, 1987; Martin and others, 1998; Tamura and others, 2008).

5. Discussion

In the previous section, we showed some evidence of the solidification of a surface slush layer resulting from accumulated snow

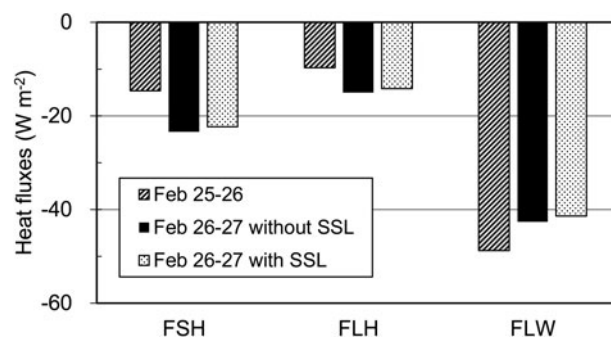


Fig. 7. Surface heat fluxes during the night, averaged from 18:00 to 06:00. FSH: sensible heat flux, FLH: latent heat flux and FLW: net longwave radiation; SSL stands for surface solidification layer.

and examined its effect on the ice growth and surface heat fluxes. Here we discuss the processes involved in more detail and its application to lake ice, based on observations.

5.1 Possible factors responsible for efficient surface slush layer solidification

In Section 4.1, we suggested that the surface slush layer solidified efficiently during the freeze-up process, judging from the additional ice thickness being comparable with the snowfall amount. It is likely that the incorporation of considerable snow particles contributed to the solidification of the surface slush layer quite effectively, presumably as a seeding effect. According to the estimated ice growth (Fig. 6a), the ice thickness before the snowfall event was only 2 mm. This thin ice layer might have acted as a collector of snow particles, which otherwise might have scattered and diluted in the sea water. Besides, very fine grain sizes ($\ll 1$ mm) of granular ice in the thin section of Figures 5b and c indicate that this snow-ice layer formed within a short time. Clearly, this fine-grained granular ice with randomly oriented *c*-axes resulted in the significantly thin-structured columnar ice through the geometric selection (Weeks and Ackley, 1986). Here we discuss why surface slush layer could solidify so effectively.

As suggested above, the seeding effect of snow particles is one of the likely factors. However, for this effect to work continuously, the latent heat generated by the freezing of sea water should be released into the air efficiently. According to Figure 6c, net longwave radiation (FLW) decreased by $\sim 40 \text{ W m}^{-2}$ soon after the main snowfall events at 20:30 on 26 February, presumably associated with the disappearance of snow clouds. Although this might have enhanced the amount of heat released from the surface slush layer which was produced by the snowfalls, it is not enough to explain the efficient solidification. This is because the heat flux needed to be released to produce a 0.01 m thick solidification layer within 1 h is estimated to be as much as 450 W m^{-2} (calculated from $\rho_i L_f \times 0.01 \text{ m} / 3600 \text{ s}$, assuming that the density of new snow is 200 kg m^{-3}). Here we would like to point out another possible contributing mechanism occurring at the microscale.

Figure 9a shows the time series of the air temperature at 0.01, 0.06 and 0.22 m above the water level at the pool site for the second night. Overall, the temporal variations are linked with each other for the three heights, like the temperature at the AWS in Figure 3a. At the same time, it is found that although the temperatures at 0.06 and 0.22 m heights were almost coincident, those at the 0.01 m height were always $\sim 1^\circ\text{C}$ higher. This indicates that a strong vertical temperature gradient was maintained near the surface during the night. To show this more clearly, we depicted the nightly averaged vertical temperature

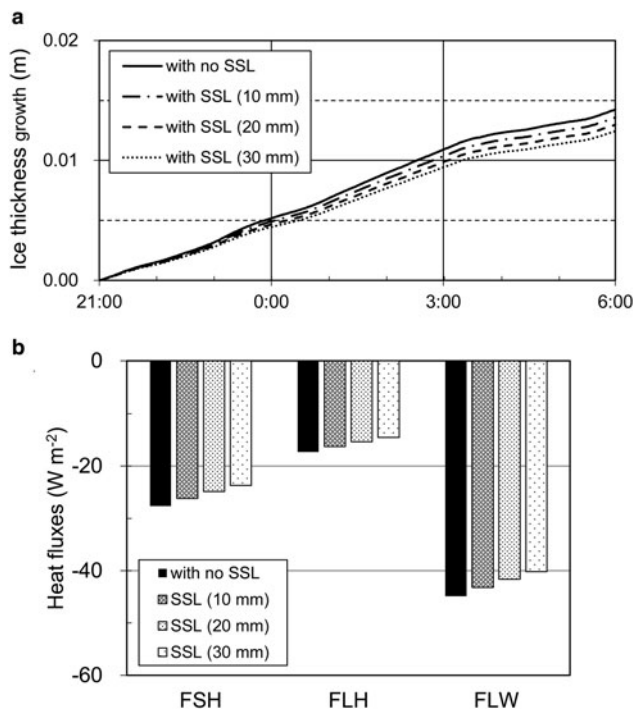


Fig. 8. The effects of snow-ice thickness (10–30 mm) on (a) ice growth after 21:00 on 26 February until 06:00 on 27 February, and (b) individual heat fluxes averaged from 21:00 on 26 February to 06:00 on 27 February. SSL stands for surface solidification layer.

profiles in Figure 9b. Although the average temperature was somewhat different between the two nights, a strong vertical temperature gradient ($\sim -22 \text{ K m}^{-1}$) is commonly found between the 0.01 and 0.06 m heights for both nights. Considering that T_s should be maintained at the freezing point (-1.7°C) when slush is present at the surface, a much stronger temperature gradient ($\sim 700 \text{ K m}^{-1}$) was maintained at the surface during the solidification of surface slush layer. Although we cannot estimate the heat flux quantitatively due to the lack of wind data on a microscale, it is likely that such a strong, persistent temperature gradient worked efficiently to release the heat generated from the surface slush layer to the air. Since the exposure of the surface slush layer to such a strong temperature gradient in the air seems to be a unique property of thin ice, it may be said that such efficient solidification of surface slush layer occurs ubiquitously when snow falls on sea ice during the freeze-up process.

Without the solidification process of the surface slush layer occurring on the microscale, it would be difficult to explain the difference of ice texture between the two nights (Figs 5a and b). On the other hand, it is noted that although the traditional 1-D thermodynamic model cannot predict this microscale freeze-up process, this process does not affect the basal freezing growth rate calculated by the model when the snowfall is less than a few centimeters. This result indicates that although the traditional thermodynamic model works well in estimating the ice production rate by basal freezing, a more sophisticated model that account for the snow–ice interaction in the atmospheric boundary layer is required to reproduce realistic ice crystal texture.

The formation of surface slush layer associated with the snow-fall event is nonetheless still puzzling. The presence of a wetted layer at the surface would increase T_s to near the freezing point. This causes two important issues. First, the vertical temperature gradient increases above the surface, which would in turn enhance the turbulent heat flux at the surface. Second, the vertical temperature gradient within the sea ice would be reduced, which would reduce the conductive heat flux within the ice. Therefore,

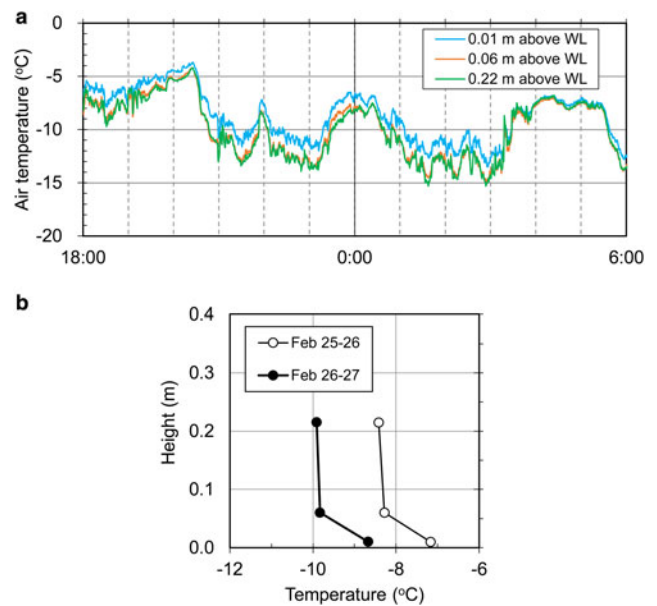


Fig. 9. Air temperatures at 0.01, 0.06 and 0.22 m above the surface at the pool. (a) Time series of air temperatures at individual heights for the second night. (b) Vertical profiles of air temperatures averaged for the first (open circle) and second (solid circle) nights.

it might be possible to reproduce this solidification layer in the 1-D thermodynamic model, if it can produce the surface slush layer. However, future work into the micro-process of surface slush layer formation is required to gain the necessary understanding to achieve this.

5.2 Solidification of surface wetted layer by wind-blown snow particles

Here, we examine the formation process of the top layer of granular ice (5 mm thick) in the thin section of Figures 5a and c. In Figure 5c, this layer is discriminated from the lower granular ice layer (10 mm thick), based on the larger grain sizes. It is interesting to note that this layer is reduced or eliminated for the sample collected near the center of the pool (Fig. 5b). It is unfortunate that we could not obtain any photographic evidence about what caused this layer from the site camera because it occurred at nighttime. For the following reasons, however, we deduce that this layer was produced through the solidification of the surface wetted layer induced by snow particles supplied by drifting snow onto the brine that has wicked to the surface of the relatively permeable ice:

- Figure 5a indicates that this layer formed after congelation ice had already grown to some extent under calm conditions with no snowfall.
- This layer appears more prominently near the margin of the pool, relative to the inner area.
- Grain sizes in this layer are relatively larger than those of the precipitation particles shown in Table 1.
- The maximum wind speed of $\sim 5 \text{ m s}^{-1}$ observed during the experiment is enough to induce drifting snow.

Item (a) can be explained only through the solidification of wetted layer on top of the sea ice. Items (b) and (c) suggest that snow particles were supplied from the surface snow surrounding the pool site, as shown by Gow and others (1990) for the Arctic leads. Item (d) is based on the past observational fact that unconsolidated snow begins to drift at a wind speed of 5 m s^{-1}

(Takeuchi, 1980; Andreas and Claffey, 1995). It is likely that the limited snow-drift transport and horizontal saltation distance of snow particles due to the relatively weak wind speed caused an inhomogeneous snow supply that was biased to the margin of the pool in the upwind direction as shown in (b). During the experiment, the maximum wind speeds ($\sim 5 \text{ m s}^{-1}$) were observed $\sim 06:00$ for the first night and at midnight for the second night (Fig. 4b). Therefore, we deduce that the main snow transport events occurred around these timings. This is consistent with the observational result, in that the uppermost solidification layer formed after the major growth of congelation ice (the first experiment) and the solidification of surface slush layer due to snowfall at 21:00 (the second experiment).

For the regions of Antarctic sea-ice cover where there are strong prevailing winds, it is suggested from observation and numerical simulation that snow loss into leads, caused by drifting snow, amounts to more than half of the total precipitation of snow on sea ice over the entire Southern Ocean (Eicken and others, 1994; Dery and Tremblay, 2004; Leonard and Maksym, 2011; Toyota and others, 2016). Our experiment showed some evidence that this process can occur ubiquitously in the polar regions where drifting snow prevails at wind speeds $> 5 \text{ m s}^{-1}$.

5.3 Application to lake ice structure

Finally, we would like to point out that our results can be applied to lake ice structure. It was noted that there are two major types of congelation ice for lake ice: (a) ice sheets composed of massive, irregularly shaped crystals with vertical c -axes and (b) ice sheets composed of vertically-elongated crystals (columnar ice) with horizontally oriented c -axes (Gow, 1986). As for the formation process of columnar ice, the possibilities of ice nucleation (frazil ice formation) under turbulent conditions (Barns and Laudise, 1985) and atmospheric seeding (frozen water droplets) under quiet conditions (Gow, 1986) were pointed out. Our results support the findings of Gow (1986). Considering that in the case of lake ice water temperature below the surface tends to be still slightly positive at the freeze-up stage, it is more likely that snow particles rather than frazil ice works to produce the initial granular ice which will thereafter grow into columnar ice underneath. Ohata and others (2016) also provide some evidence of this process from the $\delta^{18}\text{O}$ profiles of lake ice at Lake Abashiri, Hokkaido, Japan.

6. Conclusions

We conducted field experiments to grow sea ice in an artificial pool on the Saroma-ko Lagoon for two nights in February 2019 to ascertain how meteorological conditions affect sea-ice properties during the freezing process. Although the weather conditions were relatively calm during both nights, a significant snowfall event occurred on the second night. This facilitated an examination of how snowfall can affect sea-ice structure, the subsequent ice growth and the turbulent heat flux. The results from our sample analysis and a 1-D thermodynamic ice growth model are summarized as follows:

- (1) Snowfall during the freeze-up process of thin sea ice can affect the crystal alignments significantly through the solidification of a surface slush layer, which produces fine grained granular ice and thereafter thin-structured columnar ice.
- (2) Solidification of a surface slush layer during the freeze-up process has no significant effect on the subsequent ice growth (less than a few millimeters per night) and the turbulent heat flux (only a few W m^{-2} on average).

- (3) The rapid solidification of the surface slush layer is related presumably to the seeding effect of snow particle accumulation and the persistent strong temperature gradient near the surface.
- (4) A wind speed of 5 m s^{-1} appears to be sufficient to induce drifting snow and carry snow particles into leads or thin ice, resulting in solidification of the wetted layer on top of thin ice that results from brine wicking upward through the porous ice.

Item (1) provides some implications about the possibility of reconstructing the freeze-up history from thin section analysis and the understanding of the formation processes of columnar ice for lake ice. Item (2) may justify the omission of snow effects, if the snowfall amount is less than a few centimeters, in estimating the ice production rates due to bottom freezing in past polynya studies. Regarding (3), it should be kept in mind that although the traditional 1-D thermodynamic model could reproduce the bottom freezing amount well, the solidification of a surface slush layer cannot yet be predicted with this model. This indicates that we need a more sophisticated model, taking the microscale process in the atmospheric boundary layer into account. Item (4) supports the past studies about snowdrift observation and presents some evidence that wind-blown snow particles contribute to the freeze-up process of thin ice as well as snowfall.

Although these results related to the properties of granular ice induced by snowfall, we believe many of them are equally applicable to the granular ice originating from frazil ice. When frazil ice is created in sea water and then swept against the thicker ice by ocean waves under the turbulent conditions, it can accumulate under quiescent conditions that are produced due to the attenuation of waves. These have previously been referred to as a 'dead zone' (Martin and Kauffman, 1981). It is for this reason that our idealized experiments can also be applied to the harsh open water conditions of polynyas. Such surface conditions, composed of a mixture of frazil ice and sea water, would become like slush layer akin to those produced by the snowfalls in our experiments. Accordingly, the results presented in this paper could be applicable to polynyas because the solidification processes of ice crystals in sea water should be similar.

To date, the effect of snowfall on the growth of thin ice at the freeze-up process has received less attention compared with thick ice due to the logistical difficulty of field observations. Although some unique properties were revealed through our experiments, we need more field data to confirm our conclusions. Further investigation, especially the eddy flux measurement in the atmospheric boundary layer, is desirable.

Acknowledgements. This experiment was conducted as part of the Saroma-ko Lagoon Observations for sea-ice Physico-chemistry and Ecosystems 2019 program (SLOPE2019). We would like to express our sincere gratitude to Aquaculture Fishery Cooperative of Saroma Lake, Napal Kitami accommodation, and other group members of SLOPE2019 for their kind cooperation. Proof-reading by Dr Guy Darvall Williams and comments by Dr Bin Cheng, Dr Martin Vancoppenolle, and anonymous reviewers were very helpful to improve this manuscript. This work was financially supported partly by JSPS KAKENHI (#16K00511, #19K12304, #17K00534 and #18F18794).

References

- Andreas EL and Claffey KJ (1995) Air-ice drag coefficients in the western Weddell Sea. 1. Values deduced from profiles measurements. *Journal of Geophysical Research* **100**(C3), 4821–4831. doi: [10.1029/94JC02016](https://doi.org/10.1029/94JC02016).
- Aota M, Shirasawa K and Takatsuka T (1989) Measurements of an atmospheric boundary layer around the air-sea-ice observation tower: 1989 winter experiments. *Low Temperature Science, Series A* **48**, 79–89 (in Japanese with English summary).
- Bae SH, Nam JH, Sing CS and Kim C-J (2010) A numerical model for freezing drying processes with infrared radiation heating. *Numerical Heat Transfer, Part A* **58**, 333–355. doi: [10.1080/10407782.2010.508437](https://doi.org/10.1080/10407782.2010.508437).

- Barns RL and Laudise RA** (1985) Size and perfection of crystals in lake ice. *Journal of Crystal Growth* **71**(1), 104–110. doi: [10.1016/0022-0248\(85\)90049-1](https://doi.org/10.1016/0022-0248(85)90049-1).
- Dery SJ and Tremblay L-B** (2004) Modeling the effects of wind redistribution on the snow mass budget of polar sea ice. *Journal of Physical Oceanography* **34** (1), 258–271. doi: [10.1175/1520-0485\(2004\)034<0258:MTEOWR>2.0.CO;2](https://doi.org/10.1175/1520-0485(2004)034<0258:MTEOWR>2.0.CO;2).
- Eicken H, Lange MA, Hubberten H-W and Wadhams P** (1994) Characteristics and distribution patterns of snow and meteoric ice in the Weddell Sea and their contribution to the mass balance of sea ice. *Annales Geophysicae* **12**, 80–93. <https://doi.org/10.1007/s00585-994-0080-x>.
- Fichfet T and Maqueda MM** (1999) Modelling the influence of snow accumulation and snow-ice formation on the seasonal cycle of the Antarctic sea-ice cover. *Climate Dynamics* **15**, 251–268. doi: [10.1007/s003820050280](https://doi.org/10.1007/s003820050280).
- Fichfet T, Tartinville B and Goose H** (2000) Sensitivity of the Antarctic sea ice to the thermal conductivity of snow. *Geophysical Research Letters* **27**, 401–404. doi: [10.1029/1999GL002397](https://doi.org/10.1029/1999GL002397).
- Fierz C and 8 others** (2009) The International Classification for Seasonal Snow on the Ground. IHP-VII Technical Documents in Hydrology No. 83, IACS Contribution No. 1. UNESCO-IHP, Paris, p. 80.
- Frankenstein G and Garner R** (1967) Equations for determining the brine volume of sea ice from -0.5 to -22.9°C . *Journal of Glaciology* **6**(48), 943–944. <https://doi.org/10.3189/S0022143000020244>.
- Golden KM, Ackley SF and Lytle VI** (1998) The percolation phase transition in sea ice. *Science* **282**, 2238–2241. doi: [10.1126/science.282.5397.2238](https://doi.org/10.1126/science.282.5397.2238).
- Gow A** (1986) Orientation textures in ice sheets of quietly frozen lakes. *Journal of Crystal Growth* **74**, 247–258. doi: [10.1016/0022-0248\(86\)90114-4](https://doi.org/10.1016/0022-0248(86)90114-4).
- Gow A, Meese DA, Perovich DK and Tucker III WB** (1990) The anatomy of a freezing lead. *Journal of Geophysical Research* **95**, 18221–18232. doi: [10.1029/JC095iC10p18221](https://doi.org/10.1029/JC095iC10p18221).
- Granskog MA and 5 others** (2004) Chemical properties of brackish water ice in the Bothnian Bay, the Baltic Sea. *Journal of Glaciology* **50**(169), 292–302. doi: [10.3189/172756504781830079](https://doi.org/10.3189/172756504781830079).
- Hasemi T** (1974) On the growth of thin winter ice. *Low Temperature Science, Series A* **32**, 207–219 (in Japanese with English summary).
- Holtzmark BE** (1955) Insulating effect of a snow cover on the growth of young sea ice. *Arctic* **8**, 60–65.
- Ishikawa N and Kobayashi S** (1984) Experimental studies of heat budget of very thin sea ice. *Seppyo* **46**(3), 109–119 (in Japanese with English summary).
- Jutras M and 7 others** (2016) Thermodynamics of slush and snow-ice formation in the Antarctic sea-ice zone. *Deep-Sea Research Part II* **131**, 75–83. doi: [10.1016/j.dsr2.2016.03.008](https://doi.org/10.1016/j.dsr2.2016.03.008).
- Kasai T and Ono N** (1984) An experimental study of brine upward migration in thin sea ice. *Low Temperature Science, Series A* **43**, 149–155 (in Japanese with English summary).
- Kawamura T** (1982) Measurements of crystallographic orientations of sea ice. *Low Temperature Science, Series A* **41**, 173–178 (in Japanese with English summary).
- Kawamura T, Ohshima KI, Takizawa T and Ushio S** (1997) Physical, structural, and isotopic characteristics and growth processes of fast sea ice in Lutzow-Holm Bay, Antarctica. *Journal of Geophysical Research* **102**(C2), 3345–3355. doi: [10.1029/96JC03206](https://doi.org/10.1029/96JC03206).
- Leonard KC and Maksym T** (2011) The importance of wind-blown snow redistribution to snow accumulation on Bellingshausen sea ice. *Annals of Glaciology* **52**(57), 271–278. doi: [10.3189/172756411795931651](https://doi.org/10.3189/172756411795931651).
- Maksym T and Jeffries MO** (2000) A one-dimensional percolation model of flooding and snow-ice formation on Antarctic sea ice. *Journal of Geophysical Research* **105**(C11), 26,313–26,331. doi: [10.1029/2000JC900130](https://doi.org/10.1029/2000JC900130).
- Martin S** (1981) Frazil ice in rivers and oceans. *Annual Review of Fluid Mechanics* **13**, 379–397.
- Martin S, Drucker R and Yamashita K** (1998) The production of ice and dense shelf water in the Okhotsk Sea polynyas. *Journal of Geophysical Research* **103**(C12), 27771–27782. doi: [10.1029/98JC02242](https://doi.org/10.1029/98JC02242).
- Martin S and Kauffman P** (1981) A field and laboratory study of wave damping by grease ice. *Journal of Glaciology* **27**(96), 283–313. doi: [10.3189/S0022143000015392](https://doi.org/10.3189/S0022143000015392).
- Maykut GA** (1978) Energy exchange over young sea ice in the central Arctic. *Journal of Geophysical Research* **83**(C7), 3646–3658. doi: [10.1029/JC083iC07p03646](https://doi.org/10.1029/JC083iC07p03646).
- Maykut GA** (1986) The surface heat and mass balance. In Untersteiner N (ed.), *Geophysics of Sea Ice*. New York: Springer, pp. 395–463.
- Maykut GA and Untersteiner N** (1971) Some results from a time-dependent thermodynamic model of sea ice. *Journal of Geophysical Research* **76**(6), 1550–1575. doi: [10.1029/JC076i006p01550](https://doi.org/10.1029/JC076i006p01550).
- Nomura, D and 21 others** (2020) Saroma-ko Lagoon Observations for sea ice Physico-chemistry and Ecosystems 2019 (SLOPE2019). *Bulletin of Glaciological Research* **38**, 1–12. doi: [10.5331/bgr.19R02](https://doi.org/10.5331/bgr.19R02).
- Ohata Y, Toyota T and Shiraiwa T** (2016) Lake ice formation processes and thickness evolution at Lake Abashiri, Hokkaido, Japan. *Journal of Glaciology* **62**(233), 563–578. doi: [10.1017/jog.2016.57](https://doi.org/10.1017/jog.2016.57).
- Pease CH** (1987) The size of wind-driven coastal polynyas. *Journal of Geophysical Research* **92**(C7), 7049–7059. doi: [10.1029/JC092iC07p07049](https://doi.org/10.1029/JC092iC07p07049).
- Perovich DK and Richter-Menge JA** (2000) Ice growth and solar heating in springtime leads. *Journal of Geophysical Research* **105**(C3), 6541–6548. doi: [10.1029/1999JC900321](https://doi.org/10.1029/1999JC900321).
- Semtner and Jr AJ** (1976) A model for the thermodynamic growth of sea ice in numerical investigations of climate. *Journal of Physical Oceanography* **6**, 379–389. doi: [10.1175/1520-0485\(1976\)006](https://doi.org/10.1175/1520-0485(1976)006).
- Spreen G and Kern S** (2017) Methods of satellite remote sensing of sea ice. In Thomas DN ed. *Sea Ice*, 3rd Edn. Oxford, UK: John Wiley & Sons, Ltd., pp. 239–260.
- Sturm M and Massom RA** (2017) Snow in the sea ice system: friend or foe? In Thomas DN ed. *Sea Ice*, 3rd Edn. Oxford, UK: John Wiley & Sons, Ltd., pp. 65–109.
- Svensson U and Omstedt A** (1994) Simulation of supercooling and size distribution in frazil ice dynamics. *Cold Regions Science and Technology* **22**, 221–233. doi: [10.1016/0165-232X\(94\)90001-9](https://doi.org/10.1016/0165-232X(94)90001-9).
- Takeuchi M** (1980) Vertical profile and horizontal increase of drift-snow transport. *Journal of Glaciology* **26**(94), 481–492. doi: [10.3189/S0022143000010996](https://doi.org/10.3189/S0022143000010996).
- Takizawa T** (1983) Characteristics of snow cover on sea ice and formation of snow ice. *Low Temperature Science, Series A* **42**, 157–162 (in Japanese with English summary).
- Takizawa T** (1984) Characteristics of snow cover on sea ice and formation of snow ice II. *Low Temperature Science, Series A* **43**, 157–161 (in Japanese with English summary).
- Takizawa T and Wakatsuchi M** (1982) Snow layer on sea ice. *Low Temperature Science, Series A* **41**, 159–165 (in Japanese with English summary).
- Tamura T, Ohshima KI and Nishashi S** (2008) Mapping of sea ice production for Antarctic coastal polynyas. *Geophysical Research Letters* **35**, L07606. doi: [10.1029/2007GL032903](https://doi.org/10.1029/2007GL032903).
- Toyota T and 7 others** (2013) Oxygen isotope fractionation during the freezing of sea water. *Journal of Glaciology* **59**(216), 697–710. doi: [10.3189/2013JoG12J163](https://doi.org/10.3189/2013JoG12J163).
- Toyota T and 6 others** (2016) On the extraordinary snow on the sea ice off East Antarctica in late winter, 2012. *Deep-Sea Research Part II* **131**, 53–67. doi: [10.1016/j.dsr2.2016.02.003](https://doi.org/10.1016/j.dsr2.2016.02.003).
- Toyota T and Wakatsuchi M** (2001) Characteristics of the surface heat budget during the ice-growth season in the southern Sea of Okhotsk. *Annals of Glaciology* **33**, 230–223. doi: [10.3189/172756401781818400](https://doi.org/10.3189/172756401781818400).
- UNESCO (1978) Freezing point of seawater. (by Millero FJ) *Technical Papers in Marine Science* **28**, 29–35.
- Weeks WF and Ackley SF** (1986) The growth, structure, and properties of sea ice. In Untersteiner N (ed.), *The Geophysics of Sea Ice*. New York: Plenum, pp. 9–164.
- Wettlaufer JS, Worster MG and Huppert HE** (2000) Solidification of leads: theory, experiment, and field observations. *Journal of Geophysical Research* **105**(C1), 1123–1134. doi: [10.1029/1999JC900269](https://doi.org/10.1029/1999JC900269).
- Wu X, Budd WF, Lyte VI and Massom RA** (1999) The effect of snow on Antarctic sea ice simulations in a coupled atmosphere-sea ice model. *Climate Dynamics* **15**(2), 127–143. doi: [10.1007/s003820050272](https://doi.org/10.1007/s003820050272).
- Yen Y-C** (1981) Review of thermal properties of snow, ice and sea ice. *CRREL Rep.*, 81-10, 1–27.